Dynamical aspects of particle emission in binary dissipative collisions: Effects on hot-nuclei formation

Ph. Eudes, Z. Basrak,* and F. Sébille
Laboratoire SUBATECH, Université de Nantes, École des Mines de Nantes, IN2P3/CNRS, F-44 072 Nantes Cedex 03, France
(Received 25 April 1997)

Characteristics of charged-particle emission in heavy-ion reactions have been studied in the framework of the semiclassical Landau-Vlasov approach for the $^{40}Ar + {}^{27}Al$ collisions at 65 MeV/nucleon. At all impact parameters, the reaction mechanism is dominated by binary dissipative collisions. After an abundant prompt emission coming from the overlapping region between the target and the projectile, two excited nuclei, the quasitarget and the quasiprojectile, emerge from the collision. To shed some light on the role played by dynamical effects, light charged-particle observables, which are currently used as an experimental signature of a hot equilibrated nucleus, have been carefully investigated. The model calculations show that binary dissipative collisions are closely related to the so-called participant-spectator scenario in which the ''spectators,'' identified as the quasitarget and the quasiprojectile, are not very hot. [S0556-2813(97)00310-5]

PACS number(s): 25.70.−z, 24.10.−i

I. INTRODUCTION

Heavy-ion collisions are generally considered as a powerful tool for studying the properties of hot nuclear matter [1]. At relativistic energies (above 200 MeV/nucleon) the properties of hot spectators have been extensively studied [2]. At intermediate energies (20–100 MeV/nucleon), a number of recent experimental works have shown that binary dissipative collisions (BDC's) strongly dominate the reaction cross section [3–11]. The theoretical studies corroborate the binary character of these collisions [12–16]. With increasing incident energy, the incomplete fusion progressively disappears. Above the Fermi energy, it corresponds to a very small part of the reaction cross section [9,17]. Consequently, BDCs appear as being the only efficient mechanism able to produce very hot nuclear sources in this energy range.

One usually conceives the mechanism of BDCs as a two-stage process. In the first stage, the two colliding nuclei overlap and start to emit from the interaction zone. These particles are commonly identified with pre-equilibrium emission (''looking'' from the low-incident-energy side) or participant particles (looking from the high-incident-energy side). The kinematic analysis of reaction products shows an enhanced component at midrapidity, which is attributed to this early emission [18]. The collective motion of these particles (directed collective flow, azimuthal distributions) has been extensively studied since it is believed to provide information on the nuclear equation of state and in-medium effects. Several scenarios have been invoked to explain the kinematic features of midrapidity particles: nucleon-nucleon collisions, neck emission, etc. [18]. For light systems, the contribution of participant particles and/or pre-equilibrium effects are considered to be weak or even negligible [10]. This emission component has recently been studied in much detail for a heavier Xe+Sn system at 50 MeV/nucleon [18]. It has been reported that the midrapidity component may represent up to 25% of the mass of the system.

The second stage of BDC's is characterized by the formation of two excited nuclei in the reaction exit channel, generally referred to as a quasitarget (QT) and a quasiprojectile (QP). The properties of these hot nuclei (mass, velocity, excitation energy, etc.) have been extensively studied [3,4,6,7,9–12]. Owing to experimental constraints, most of these studies have been performed only for the fast source, namely, the QP. The experimental procedure allowing one to derive the properties of the hot nucleus can be summarized as follows. The angular distribution of the particles located in the forward hemisphere of the QP reference frame shows a behavior very close to what is expected for the emission from an equilibrated source. All these particles are then assumed as being emitted by a hot equilibrated primary quasiprojectile. By following such a scenario, the reconstructed mass of the hot nucleus is found to be close to the projectile mass with a weak dependence on the impact parameter and the incident energy [6,7,9–11,19]. For light systems, the excitation energies exceeding 10 MeV per nucleon have been reported [6,9–11,19].

BDC's are a typical transition-energy-region phenomenon and may be viewed, following one's own sensibility, as either an evolution of the low-energy deep-inelastic process [20] or the first fruits of the high-energy participant-spectator picture [21]. The main difference between these two approaches concerns the participant emission in both its amount and its physical origin. The aim of the present work is to derive the properties of BDC's by carefully studying the dynamical aspects of these collisions. We address the above question theoretically by confronting the results of a simulation with a semiclassical dynamical model, the Landau-Vlasov model (LVM), against the experimental results. The advantage of dynamical models is the straightforward analysis of time evolution of any observable and the possibility of focusing attention to any subset of particles (say, only to those originating from the target). The LVM correctly pre-

*On leave from Ruđer Bošković Institute, HR-10 001 Zagreb, Croatia.

dicts the average behavior of particle emission and, in particular, of those observables that are frequently used in the analysis of experimental data to infer on the formation (existence) of a hot nucleus. This *a posteriori* justifies the conclusions to be drawn on the dissipation of the initial energy as well as on the dynamics of the reaction.

In this paper we have chosen to investigate the Ar+Al collision at 65 MeV/nucleon, a system that has been extensively studied experimentally [9,22–30]. The theoretical model used for the simulation is briefly reviewed in Sec. II. The nature of the reaction mechanism governing the collision is globally discussed in Sec. III. Section IV is devoted to the study of the characteristics of emitted particles by detailed analyses of the phase space being at the origin of the emission of particles emitted during the different stages of the reaction. In the early stage of the collision we obtain a hot compact composite nucleus that emits copiously (prompt emission coming from the interaction zone). This composite nucleus breaks into the QT and the QP. In Sec. V we show that the picture of a hot nucleus formed in BDC's that we draw from our dynamical calculations markedly differs from that stemming from experimental studies: the QT and the QP are not strongly excited when they separate. Our conclusions are summarized in Sec. VI.

II. OUTLINE OF THE MODEL

Let us briefly recall the properties of the Landau-Vlasov (LV) equation, which governs the time evolution of the one-body distribution function $f(\vec{r},\vec{p};t)$:

$$\frac{\partial f}{\partial t}+\left(\frac{p}{m}+\frac{\partial U}{\partial p}\right)\frac{\partial f}{\partial r}-\frac{\partial U}{\partial r}\frac{\partial f}{\partial p}=I_{\mathrm{coll}}(f), \tag{2.1}$$

where $U(\vec{r},\vec{p};t)$ is the self-consistent mean field in the Wigner representation and $I_{\mathrm{coll}}(f)$ is the collision integral calculated in the Uehling-Uhlenbeck approximation. This collision term reads

$$\begin{aligned} I_{\mathrm{coll}}=&\frac{g}{4m^2}\frac{1}{\pi^3\hbar^3}\int d\vec{p}_2 d\vec{p}_3 d\vec{p}_4 \frac{d\sigma}{d\Omega}\delta(\vec{p}+\vec{p}_2-\vec{p}_3-\vec{p}_4)\\ &\times\delta(p^2+{p_2}^2-{p_3}^2-{p_4}^2)[(1-\overline{f})(1-\overline{f_2})f_3 f_4\\ &-(1-\overline{f_3})(1-\overline{f_4})f_2 f], \end{aligned} \tag{2.2}$$

where σ is the free nucleon-nucleon cross section, chosen to be isotropic and with its usual energy and isospin dependence, $\overline{f}=(2\pi\hbar)^3 f(\vec{r},\vec{p};t)/g$ is the occupation number, g is the degeneracy, and m is the nucleon mass. The LV equation is solved for a nonlocal effective force (Gogny D1-G1) [31,32] by expanding the distribution function $f(\vec{r},\vec{p};t)$ on the basis of coherent states g_χ and g_ϕ that follow semiclassical trajectories in phase space [31,33]:

$$f(\vec{r},\vec{p};t)=\frac{A}{N}\sum_i \omega_i(\vec{r}_i,\vec{p}_i)g_\chi(\vec{r}-\vec{r}_i(t))g_\phi(\vec{p}-\vec{p}_i(t)). \tag{2.3}$$

In Eq. (2.3), A is the system mass number, N is the number of coherent states, actually a basis of Gaussians, and w_i's are weight factors [34]. According to Ref. [35], the ratio N/A has been fixed in order to minimize fluctuations in global observables. In our particular case, the optimal ratio corresponds to about 100 coherent states per nucleon.

Within the one-body approximation, the distinction between coherent states bound in a nucleus and those that have already left it (referred to as *emitted* or *free particles*, i.e., Gaussians) constitutes a conceptual difficulty. However, let us consider the part of the colliding system for which the local spatial density is higher than the threshold $\rho_0/8$, ρ_0 being the normal nuclear density as forming a massive cluster. The rest of the system constitutes the ensemble of emitted particles. In order to approach the mass values of cold residues close to the values observed experimentally, all simulations have been carried out up to 800 fm/c. Owing to the unavoidable incompleteness of the phase-space sampling, spurious nucleon evaporation occurs. Recent studies [36] have shown that owing to the spurious evaporation, the number of emitted nucleons does not exceed 5% for times as long as 1000 fm/c. Beyond 800 fm/c, the calculation has been continued until 8000 fm/c considering only the Coulomb repulsion due to reaction residues in order to achieve the correct asymptotic directions of emission.

One-body approaches cannot give but the global description of the emission with no insight into the relative abundance of various charge states. On the other hand, in the model considered, at each time step of simulation one readily calculates the physical properties of the system as a whole or separately the properties of heavy remnant(s) or free particles. Thus the calculation gives the average behavior of reaction products and allows a close followup of their time evolution. The simulation is performed at five impact parameters ranging from $b=0.5$ fm (central collisions with full overlap) to $b=6.5$ fm (peripheral collisions with less than 3 fm overlap between the projectile and the target).

III. REACTION MECHANISM AND CHARACTERISTIC TIMES OF THE REACTION

The simulated time evolution of density profiles for the two impact parameters representative of the central ($b=0.5$ fm) and semiperipheral ($b=5$ fm) collisions are displayed in columns (a) and (d) of Fig. 1. The contour plots are obtained by projecting the density onto the reaction plane (x,z), z being the beam direction. Two residual nuclei are present in the exit channel at all impact parameters. For the most central collisions ($b=0.5$ fm), the lighter partner (target) vaporizes, although clearly keeping the memory of the entrance channel. This is exemplified by columns (b) and (c), which show density profiles of particles belonging initially to the target [column (b)] and to the projectile [column (c)], respectively. Although part of particles is transferred from the projectile to the QT and from the target to the QP, their densities are too small to be observed in the figure (see also Table I). Finally, let us notice that the LVM dynamical simulation does not predict formation of a fusionlike residue, in full accordance with the experiment [9].

To simplify the followup of the evolution of emitted particles arising from different dynamical contributions, let us define the times that characterize the distinct stages of the reaction. The first one, labeled t_{PE}, is defined as the time at

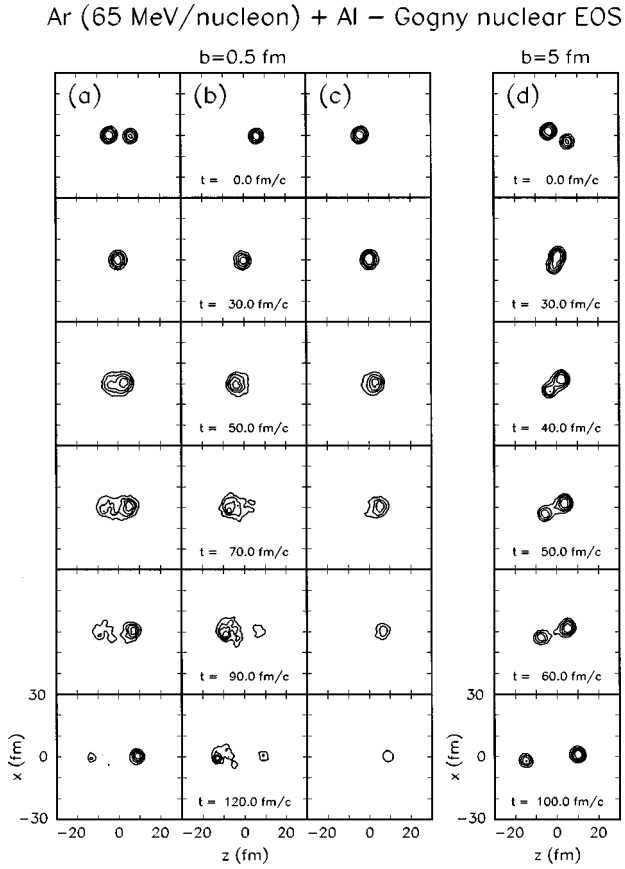

FIG. 1. Time evolution of the equidistant density-profile contours projected onto the reaction plane for $b=0.5$ fm [columns (a)–(c)] and $b=5$ fm [column (d)]. Columns (b) and (c) show the density profiles of the particles belonging initially to the target and to the projectile, respectively. The z axis is along the projectile direction.

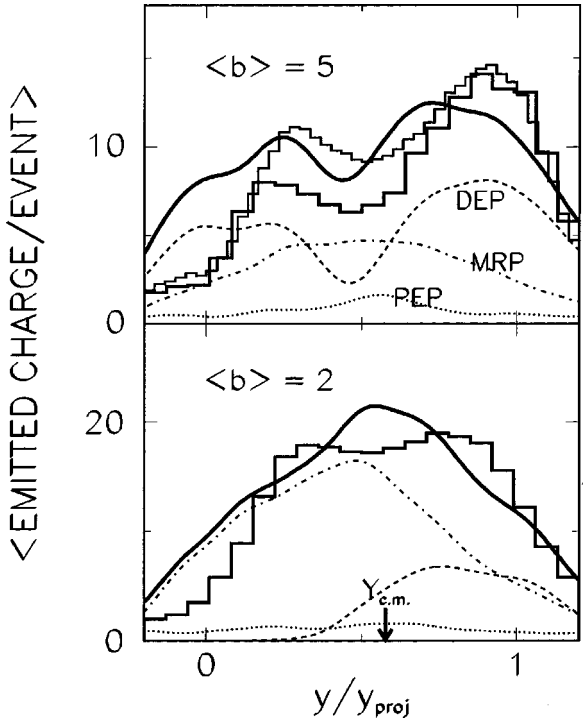

FIG. 2. Charged-particle rapidity distributions for $b=2$ fm (bottom) and $b=5$ fm (top) collisions. Curves represent the results of simulation at t_∞ and histograms are obtained by summing up experimental $Z=1$ and $Z=2$ distributions for the same estimated mean values of b. The thin and heavy histograms in the upper panel are due to the two different event-sorting procedures. Dotted curves show the distribution of particles emitted before t_{PE}, dash-dotted curves for $t_{\mathrm{PE}}<t<t_{\mathrm{sep}}$ emission, dashed curves for delayed emission ($t>t_{\mathrm{sep}}$), and heavy solid curves the global distribution of all emitted charged particles. The particle rapidity y is normalized by the projectile rapidity y_{proj}. Zero stands at the target rapidity and unity at the projectile rapidity. The c.m. rapidity is marked by an arrow labeled $Y_{\mathrm{c.m.}}$.

which the total momentum distribution becomes locally spherical (for more details see Ref. [37]). For this system and at the energy studied, one finds that t_{PE} shows no dependence on the impact parameter and is equal to about 30–35 fm/c. In most of theoretical models, particles emitted prior to t_{PE} are considered as pre-equilibrium particles and will afterwards be labeled as PEP's (pre-equilibrium particles). Columns (a) and (d) show that at this time the system forms a single compact nucleus. The system has just gone through the maximal compression whose value is strongly b dependent. The second characteristic time, labeled t_{sep}, is the time at which the dumbbell-like configuration breaks at its neck into two excited nuclei, the QT and the QP, which, after separation, travel apart from each other in the configuration space. Hereafter, we call them the primary QT (PQT) and primary QP (PQP). For our system at the studied energy, t_{sep} weakly varies with impact parameter and takes in peripheral collisions ($b=6.5$ fm) about 50 fm/c and regularly increases to attain about 80 fm/c in central collisions. Between t_{PE} and t_{sep}, the system evolves rapidly in both the configuration and the impulse space. The system has a more or less compact dinuclear shape and emits around midrapidity. Therefore, we label particles emitted for $t_{\mathrm{PE}}<t<t_{\mathrm{sep}}$ midrapidity particles (MRP's). Before t_{sep} the system emits copiously and MRP's together with PEP's form a set of prompt particles (PRP's). After t_{sep} the hot PQT and PQP emit slowly much like the sequential evaporation process. We call these particles the delayed particles (DEP's). The time at which we stop the dynamical calculation is $t_{\mathrm{end}}=800$ fm/c and it has only technical meaning. For charged particles emitted in a given time interval, the behavior of studied observables changes appreciably with time. The nuclear mean field has negligible influence on free particles. Consequently, the experienced evolution of properties for particles belonging to the same dynamical subset must be the exclusive effect of the Coulomb interaction. To underline this evolution, throughout the present paper, some observables are shown for a given particle group at the end of the time interval in which they were emitted, i.e., t_{PE}, t_{sep}, t_{end}, and also for the asymptotic time

TABLE I. Percentage of original target nucleons in PQT, PQP, and amongst PRP's as a function of b.

b	0.5	2.0	3.5	5.0	6.5
PQT	78.1	80.3	90.4	91.8	96.1
PQP	11.7	9.8	8.4	4.7	3.1
PRP	49.8	54.6	52.7	48.3	51.6

$t_\infty = 8000$ fm/c. To avoid ambiguities, this time will be noted by $t^\infty_{\rm PE}$, $t^\infty_{\rm sep}$, and $t^\infty_{\rm end}$ for each of particle groups.

IV. CHARACTERISTICS OF EMITTED PARTICLES

A. Rapidity distributions

In Fig. 2 the summed experimental rapidity distributions for particles of charges $Z=1$ and 2 are shown as histograms for the estimated experimental impact parameters $b=2$ (bottom) and 4.5 fm (top) [30,38]. The solid curves in Fig. 2 show the rapidity distributions for $b=2$ and 5 fm calculated at t_∞. At semiperipheral impact parameters two contributions centered around QT and QP rapidity are distinctly seen and they differ from the distribution sitting at the c.m. rapidity. For more central collisions, the three contributions strongly overlap since the QT and the QP get gradually closer to the c.m. rapidity as b decreases because of the growing stopping power of the collision. The integrated values of calculated and measured distributions are about the same, but the simulation does not reproduce each detail of experimental distributions. The reasons may be (i) neglect of the experimental filter that imposes relatively high particle-velocity detection thresholds [39,40], (ii) mixing of $Z=1$ and 2 contributions, which, owing to substantially different Coulomb effects, display different dependence on rapidity [30,38], and, finally, (iii) the rapidity distributions are strongly b dependent. The impact parameter cannot be accurately determined in a measured event [41]. To exemplify it, Fig. 2 shows the rapidity distributions for the same estimated experimental impact parameter $b=4.5$ fm but obtained using two different event-sorting procedures [30,38]. The mixed contribution of a range of impact parameters tends to enlarge and wash out the existing structure of the distribution. Despite the above discrepancies, the LVM provides a correct description of measured rapidity distributions. In addition, the model allows unfolding of the PRP and the DEP contributions. From the dotted curves it follows that PEP's are spread over the whole available rapidity range. The MRP's are dominantly sitting at midrapidity (dash-dotted curves), whereas DEP's, being emitted from the QT and the QP, are centered around the QT and QP rapidity (dashed curves).

B. Multiplicity of charged particles

In the preceding subsection it was shown that the total, i.e., rapidity-integrated, emitted charge is rather well predicted by the calculation. In our one-body approach, each particle carries the same charge, so that the total emitted charge is equivalent to the multiplicity of charged particles. This quantity is shown in Fig. 3 as a function of the impact parameter. As expected, the total multiplicity increases steadily with the violence of collision (filled circles and solid line). It displays a close-to-linear dependence on b and does not saturate with centrality. Such behavior results from presenting the total charge and not the true particle multiplicity of particles of various charge states. The PEP's display a weak dependence on b and represent at most about 10% of the total emitted charge (open triangles and dotted line). Most of the particles are emitted between $t_{\rm PE}$ and $t_{\rm sep}$ (open circles and dash-dotted line) when the system rapidly evolves from a compact to a dumbbell-like dinuclear shape

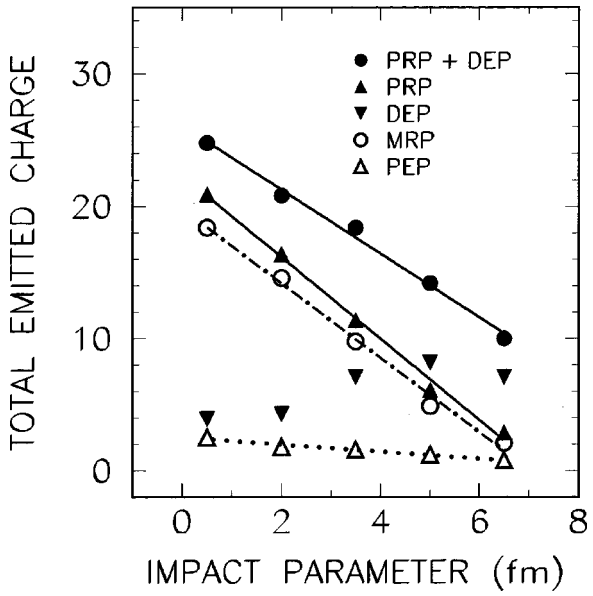

FIG. 3. Calculated multiplicity of emitted charged particles for various particle groups as a function of b. Presented are particles emitted before $t_{\rm PE}$ (dotted line and open triangles), emitted between $t_{\rm PE}$ and $t_{\rm sep}$ (dash-dotted line and open circles), all prompt emission with $t<t_{\rm sep}$ (solid line and filled triangles), and emitted after $t_{\rm sep}$ (delayed emission; filled inverted triangles). The summed contribution of prompt and delayed components is shown as solid line and filled circles.

and reaches the global relaxation in momentum space (see, e.g., Fig. 1 in Ref. [42]). The prompt emission dominates central and semicentral collisions. Like the total emission, it strongly increases with centrality, displaying an almost linear dependence on b (filled triangles and solid line). Since PEP's display a weak dependence on b, for peripheral collisions they represent more than one-quarter of the PRP's. Contrary to the prompt emission, the delayed emission shows a weak dependence on b, reaching its maximum for semicentral collisions (filled inverted triangles). This component dominates peripheral collisions, but, generally speaking, represents a relatively small portion of the total emitted charge. This is due to the substantial dissipation of the transferred entrance-channel energy at the reaction stage characterized by a composite dinucleus ($t<t_{\rm sep}$). Taking the above results at their face value, our model calculations suggest that the PQT and PQP are not very hot nuclei.

C. Invariant cross section of charged particles

1. Global emission

In order to identify the emission sources in an experiment, one frequently resorts to the two-dimensional presentation of data via invariant cross sections $\sigma_{\rm inv}=d^2\sigma/p_\perp dp_\perp dp_\parallel$. The eventual existence of binary processes is straightforwardly inferred from these plots. Therefore, to strengthen our conclusions drawn from the study of rapidity distributions, in Fig. 4 we display invariant cross sections for the simulation of the most central ($b=0.5$ fm, top), intermediate ($b=3.5$ fm, middle), and the most peripheral ($b=6.5$ fm, bottom) studied collisions. This choice makes transparent the evolution with centrality of the emission pattern and of the under-

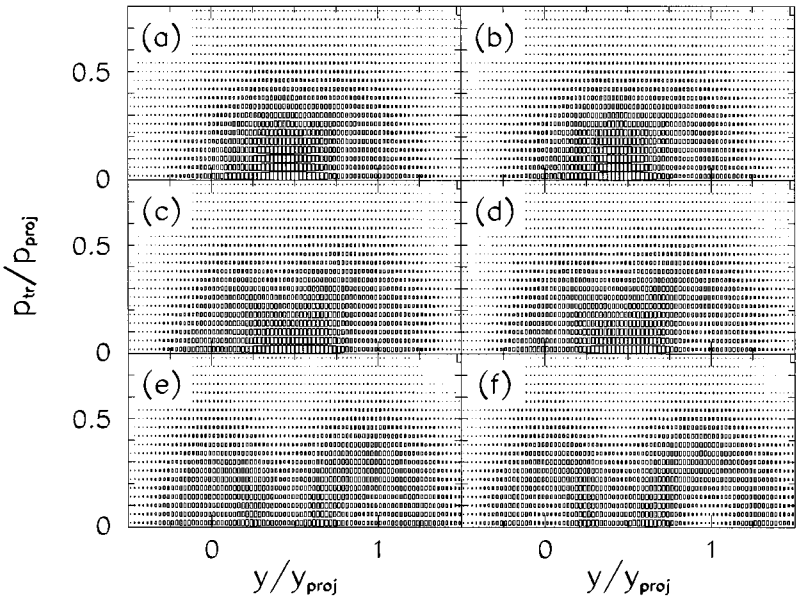

FIG. 4. Calculated invariant cross sections for all emitted charged particles for $b=0.5$ fm (top), $b=3.5$ fm (middle), and $b=6.5$ fm (bottom) collisions. Left-side panels refer to calculations performed at $t_{\rm end}$ and right-side ones at $t_{\rm end}^{\infty}$.

lying Coulomb effects. In the figure, the longitudinal momentum is expressed by the relative rapidity $y=y_i/y_{\rm proj}$, i.e., the particle rapidity normalized by the projectile rapidity. (At the energy considered $y\approx\beta=v/c$.) Similarly, the transverse momenta are expressed per nucleon and normalized by the projectile momentum. The left-side panels refer to calculations performed at the end of the full dynamical calculation $t_{\rm end}$, whereas the right-side panels refer to calculations at the time $t_{\rm end}^{\infty}$. At $t_{\rm end}$ one observes two outstanding sources for peripheral collision: the slow source close to the target rapidity that is associated with the emission from the QT and the fast one close to the projectile rapidity associated with the QP. The emission pattern is marked by the strong ringlike structure around each source. These rings are caused by the repulsive Coulomb effect that depopulates the zones of the $(p_{\parallel},p_{\perp})$ plane around the emission sources (heavy reaction remnants). The emission displays a high degree of isotropy for each source. For decreasing impact parameters, these two sources get progressively closer to each other (smaller recoil velocities of remnants) and finally overlap substantially: In the central collision studied, a single midrapidity source dominates a fairly isotropic emission pattern. The Coulomb rings fade out with centrality owing to both ever closer (growing stopping power) and ever less massive (growing violence of the collision) QT and QP which exercise a weaker Coulomb repulsion on emitted particles. The two main Coulomb rings extend to the midrapidity region, which becomes more and more filled. In Sec. IV C 3 it will be shown that an authentic midrapidity emission is present at every impact parameter, but its strength is strongly b dependent.

By comparing the left-side with the right-side panels, one observes that the Coulomb ringlike pattern gets somewhat enhanced by the Coulomb continuation of the dynamics. Careful scrutiny of Fig. 4(a) and, particularly, of Fig. 4(b) reveals the existence of a weak Coulomb ring in central collisions on the projectile side. Owing to the disappearance of the QT remnant in central collisions, the corresponding Coulomb ring cannot be discerned on the target side.

Since the experimental $\sigma_{\rm inv}$ plots exhibit drastic differences for $Z=1,2,3$–5 and $Z\geqslant 6$ charges [9], a direct comparison with experimental yields is not possible. $Z=1$ and 2 species dominate the reaction cross section and one may limit the comparison only to those data. Qualitatively, the experiment and the LVM simulation display the same general behavior with three distinct sources.

At this point it is instructive to examine the history of the emitted particles, group by group, for every reaction phase. To make transparent the dynamical effects and the binary character of this reaction, we show emission patterns not only for the full emission group (PEP's, MRP's, and DEP's), but also separately for the original target and projectile particles, both at the end of the emission of a given group and at t_{∞}. We show the invariant cross sections only for the $b=3.5$ fm yields. Similar conclusions can be drawn for every impact parameter.

2. Pre-equilibrium particles

Figure 5 displays the calculated invariant cross sections of charged PEP's at $b=3.5$ fm. $\sigma_{\rm inv}$ is presented at $t_{\rm PE}=35$ fm/c (left), i.e., just after the pre-equilibrium emission has ceased and for the very same particles but at the asymptotic time $t_{\rm PE}^{\infty}$ (right). The figure shows particles originating from the target (top), the projectile (middle), and all PEP's, i.e., sum of both (bottom). As commonly expected for the pre-equilibrium emission, at $t_{\rm PE}^{\infty}$ one observes the strongly localized emission around the target rapidity, the midrapidity, and the projectile rapidity, respectively (bottom right). One notices that the target-side component is stronger than the projectile one, the former being fed exclusively by the target (top) and the latter by the projectile (middle). This supports the picture of inertial pre-equilibrium emission in which these particles are preferentially emitted by the lighter partner. The observed behavior reminds one of the so-called

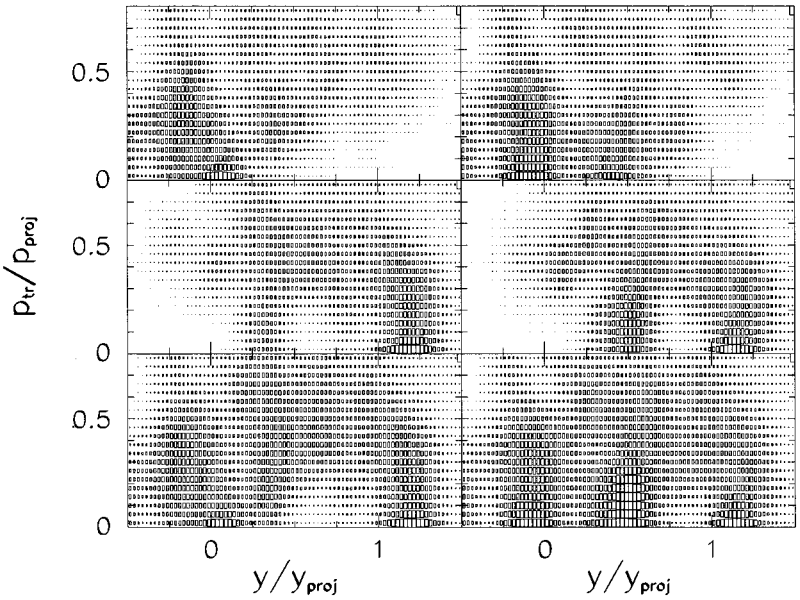

FIG. 5. Calculated invariant cross sections for pre-equilibrium charged particles at $b=3.5$ fm. Particles belonging initially to the target (top), the projectile (middle), and for all PEP's (bottom) are shown separately. The left column refers to calculations performed at the end of emission ($t<t_{\mathrm{PE}}$), i.e., at t_{PE}, and the right one for the same particles but at t_{PE}^{∞}. All panels have a common normalization.

Fermi-jet emission. The QT and QP rapidity zones are strongly depopulated for all transverse momenta. One may, however, observe a high strength of the transversal component in the whole rapidity range.

The midrapidity component appears as the strongest one. It is commonly identified as genuine pre-equilibrium emission consisting of fully stopped particles undergoing a single elastic nucleon-nucleon (target-projectile) collision that ejects them outside the attractive potential of the bulk. Such a scenario is not fully supported by our LVM simulation. In the calculation, at t_{PE} (left column of Fig. 5), nucleon-nucleon collisions induce a broad and somewhat irregular distribution around midrapidity. This component, which is not well structured at t_{PE}, becomes the main component of PEP's emission at t_{PE}^{∞}. It is, under the Coulomb force, strongly squeezed around midrapidity and slightly pushed towards the target side owing to the stronger QP Coulomb field.

The above result has significant consequences. On the one hand, it shows the importance of the Coulomb field for the final distribution of PEP's, and, on the other hand, underlines the impossibility of disentangling the pre-equilibrium component from the rest of the emission in an experimental distribution. Namely, if one compares the plots obtained at t_{∞} for the global emission of charged particles [Fig. 4(d)] with the plot of PEP's (bottom right in Fig. 5), one concludes that they are entirely mixed, in particular at midrapidity. One has to keep in mind, however, that the number of PEP's is small (see Figs. 2 and 3).

3. Particles emitted between t_{PE} and t_{sep}

Particles emitted between $t_{\mathrm{PE}}=35$ fm/c and $t_{\mathrm{sep}}=70$ fm/c (MRPs) increasingly dominate the overall emission as the impact parameter decreases (cf. Fig. 3). Careful study of this group of particles is of prime interest because they carry the key of the understanding whether BDC's have to be viewed as an extension of the low-energy phenomena (deep inelastic collisions) or as the first fruits of the high-energy participant-spectator picture. More precisely, the underlying question is whether we must consider MRP's as participant emission coming from the interaction zone or as a very early emission coming from PQT and PQP, before they appear in the configuration space. The latter picture implies the compact composite dinucleus created in the early stage of the collision as being formed of two independent quasiequilibrated nuclei. A first indication of an answer to this question can be found in Fig. 6, which displays the calculated σ_{inv} of MRP's at the separation time t_{sep} (left) and at $t_{\mathrm{sep}}^{\infty}$ (right). At t_{sep}, the total MRP's emission (bottom) appears as a single-source pattern centered at midrapidity. Moreover, these particles extend over the whole rapidity range accessible in the collision. In particular, MRP's fill rather homogeneously the high-rapidity zone. In the QP reference frame, these particles exhibit a strange regularity, which is somewhat enhanced at $t_{\mathrm{sep}}^{\infty}$ by the Coulomb effects (see Sec. V A). At $t_{\mathrm{sep}}^{\infty}$ the Coulomb field of QT and QP somewhat distorts this one-source pattern by squeezing particles to the c.m. rapidity and by slightly depopulating the QT and QP surroundings. One does not observe the expected behavior for a two-sources-emission process; it would be characterized by a clear ringlike structure around the QT and QP rapidity. The above picture evolves slowly with b owing to the changing strength of the QT and QP Coulomb field from peripheral to central collisions.

A stronger argument can be drawn from Fig. 7. The trajectories of MRP's are followed backward in time to derive their exact origins in phase space (right). The configuration space is shown in the upper and the impulse space in the lower panel. For the sake of comparison, respective plots for the whole system are shown on the left side. Unambiguously,

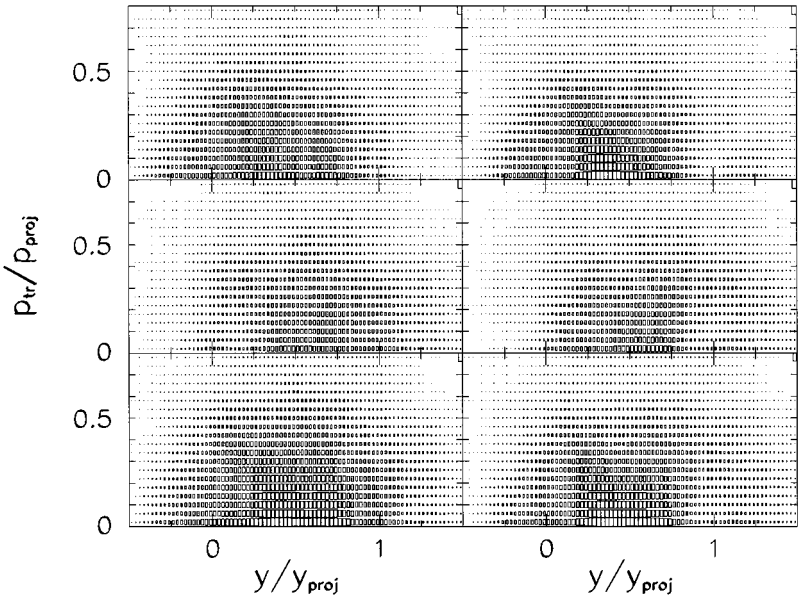

FIG. 6. Same as Fig. 5 but for MRP's, i.e., for particles emitted in the interval $t_{PE}<t<t_{sep}$ at t_{sep} (left) and at t_{sep}^{∞} (right).

the MRP's originate from the interaction zone (top) and are vigorously confined at midrapidity prior to emission (bottom). This analysis argues in favor of the participant-spectator picture.

4. Delayed particles

Figure 8 displays the calculated invariant cross sections for particles emitted between $t_{sep}=70$ fm/c and $t_{end}=800$ fm/c at the end of the dynamical calculation, i.e., at t_{end} (left) and at t_{end}^{∞} (right). Owing to the conspicuous ringlike structure, the two emitting sources, the QT and QP, show up nicely. In addition, the top and middle panels admirably show a very limited transfer of matter between the target and the projectile, which reminds us of the spectator nuclei of the high-energy participant-spectator picture. The amount of the original target particles in PQT, PQP, and amongst PRP's is given in Table I as a function of b. The target particles amount to 40.3% of the system mass. The regular isotropic distribution speaks in favor of evaporationlike emission. Indeed, the emission process suddenly changes after the separation of PQT and PQP. Whereas the emission between t_{PE} and t_{sep} is tempestuous (high emission rate up to 0.8 nucleons per fm/c), it is, after separation, rather calm and the emission rate does not exceed 0.03 nucleons per fm/c (for $b=5$ fm, see also Fig. 2 in Ref. [42]). The enhanced QP emission on the low-rapidity side is probably due to the contribution of the so-called neck emission. When the massive composite dinucleus breaks into PQT and PQP, the neck formed between them is mostly vaporized and this phenomenon is asymmetric about the c.m. for our asymmetric system. It is not obvious to which group of particles the neck emission may be associated, but we did not want to consider it apart as a distinct emission group. Let us mention that very recent experimental invariant cross sections of the Xe+Sn reaction at 50 MeV/nucleon exhibit a similar low-rapidity-side enhanced QP emission from semicentral to peripheral collisions [43]. The Coulomb extra push, which depopulates the zone at the source neighborhood, enhances the ringlike structure at t_{end}^{∞}.

D. Discussion of charged-particle emission

The results on emitted particles presented above are in fair agreement with the experiment [9,28,30,38]. In particular, both the density profiles (Fig. 1) and the invariant cross sections (Figs. 4–6, and 8) demonstrate the binary character of the reaction, in full agreement with experiment [9]. The quality of model predictions bears out the conclusion that a great portion of particles (MRP's) come from the contact region between the two interacting nuclei (the interaction zone) and are emitted promptly from the composite dinucleus formed in the early stage of the collision. In the following section we study the QP properties more specifically and analyze what effects such an ample prompt emission produces on the formation of hot nuclei in BDC's.

V. STUDY OF THE QUASIPROJECTILE

Should one create very hot nuclei in dissipative heavy-ion binary reaction channels, this will be evidenced experimentally via QP properties [1]. In an experiment, however, one cannot have direct access to the information on the properties of a hot nucleus; one has to reconstruct it by analyzing the reaction products. At the energy considered and for the system studied, light particles are of particular interest because they strongly dominate the reaction. Several experimental observables, such as multiplicity of decay products, their nature, kinetic energy spectra, and angular distributions, are currently considered, so as to provide information on hot primary nucleus formed in a heavy-ion collision. Our goal is twofold. (i) We aim to reproduce the experimental results as closely as possible. By confirming the ability of the LVM simulations in this way, (ii) we are going to analyze the

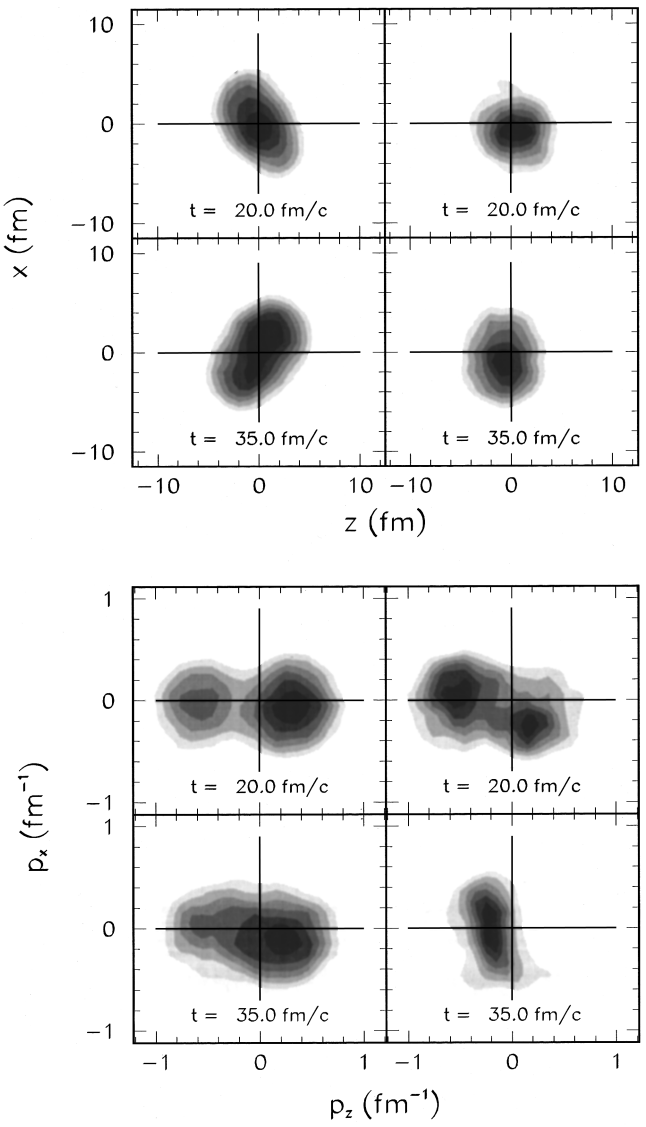

FIG. 7. Equidistant density-profile contours projected onto the reaction plane for $b=3.5$ fm at the time of maximal compression (20 fm/c) and at $t_{\mathrm{PE}}=35$ fm/c, i.e., at the time at which the emission of MRPs starts. Shown are density profiles in both the configuration (top) and the impulse space (bottom) and for the whole system (left) and, exclusively, for the MRP's (right).

dynamical fingerprints in the formation of hot nuclei via BDC's. In studying the features of the QP, we follow the *calorimetric* procedure adopted by Cussol *et al.* [28] and Péter *et al.* [9] in analyzing their experimental data. Despite the fact that the simulated collision, when analyzed strictly in the same way as the experimental data, closely reproduces the observables that have been used to conclude on the existence of very hot PQP, we draw a different conclusion regarding the formation of very hot nuclei.

A. Angular distributions

In an experiment, the calorimetric reconstruction of the PQP properties (mass and/or charge, excitation energy, etc.) consists in summing up the contribution of the detected charged particles plus the estimated contribution of undetected neutrons that are assumed to be emitted by PQP. To avoid the contamination from the non-PQP sources, one integrates particles emitted into the forward hemisphere of the QP reference frame and multiplies the obtained result by 2. The underlying presumption is that PQP emits isotropically (equilibrated source).

Proceeding in this way, the velocity of the emission source $\vec{v}_{\mathrm{QP}}$ is the first parameter to be determined. Several methods of the analysis of the available experimental data have been used to determine the $\vec{v}_{\mathrm{QP}}$ of the QP residue. Nowadays, the $\vec{v}_{\mathrm{QP}}$ vector is currently inferred from an event-by-event basis [9–11,18,28,44].

One has to prove that the PQP can be considered as an equilibrated source. Since the experimental angular distributions exhibit fairly constant behavior between 0° and 90°, it has been concluded that the source (PQP) is in thermal equilibrium.

The calculated angular distributions display the same feature. For all impact parameters (solid histograms in Fig. 9) it happens that the angular distributions between 0° and 90° are compatible with the emission from an equilibrated hot nucleus. Contrary to the significant presumption of the analysis of experimental data, in the LVM simulation this part of phase space is fed not only by DEP's, but also by PRP's. Indeed, the emission prior to the separation of PQT and PQP calculated at $t_{\mathrm{sep}}^{\infty}$ represents a non-negligible component at all impact parameters (Fig. 9, dotted histograms). Besides dominating the global emission in central collisions (see Fig. 3) for the same b's, this component also strongly dominates the emission into the forward 2π of the QP reference frame. Surprisingly enough, below 90° the combined contribution of PEP's and MRP's in the QP reference frame displays a rather flat behavior (see also Sec. IV C 3). The PRP angular distributions exhibit a significant rise for $\theta>90°$. The observed rise is mainly due to the fact that the QP is not the proper reference frame for these particles, but it is caused also by the neck emission and its squeeze around midrapidity by the Coulomb effect (see Fig. 6). In central collisions, the DEP component displays a perfectly flat angular distribution (bottom of Fig. 9, dashed histogram). At $b=5$ fm the backward rise is present and is mainly due to the contamination from the neck emission, though the contribution from the QT emission (nonexisting component in central collisions) cannot be ruled out either (see Fig. 8). The simulation shows that the nearly isotropic emission into the forward 2π QP space is a necessary but not sufficient condition for the existence of a unique equilibrated source.

B. Reconstructed PQP emission

In spite of the above criticism, let us process the results of the LVM simulation in the same way as it has been done in the analysis of the experimental data [9,28]. If all these particles were emitted from the PQP, twice the integral of angular distributions between 0° and 90° (hatched area in Fig. 9) would give the total emitted charge from the presumed PQP. The result obtained is displayed as filled circles in Fig. 10. The hatched area in Fig. 10 represents the reconstructed experimental emission from the PQP [9]. Under the conditions of the analysis discussed above, the calculation agrees favorably well with the experimental total emitted charge.

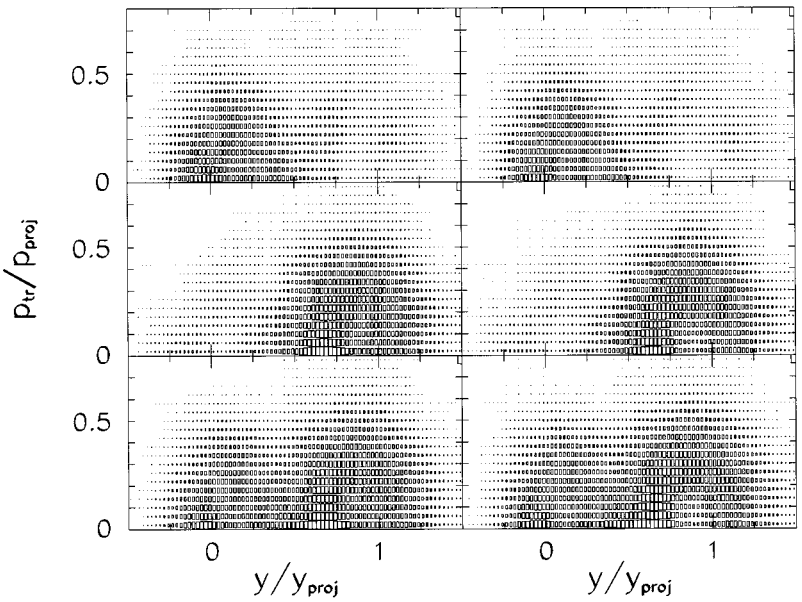

FIG. 8. Same as Fig. 5 but for DEP's, i.e., for particles emitted in the interval $t_{sep}<t<t_{end}$ at t_{end} (left) and at t_{end}^{∞} (right).

Figure 10 also displays separate reconstructed multiplicities of PRP's (open circles) and DEP's (filled inverted triangles). The PRP's, originating from the interaction zone, dominate the reconstructed central-collision multiplicity and exhibit an almost linear rise with centrality. The PEP are not shown, but this component, as for the global emission (see Fig. 3), is weak and represents 10% (peripheral collisions) to 15% (central collisions) of the total reconstructed multiplicity. Its relative contribution in forward PRP's grows, however, faster with b than for the global emission since the mid-

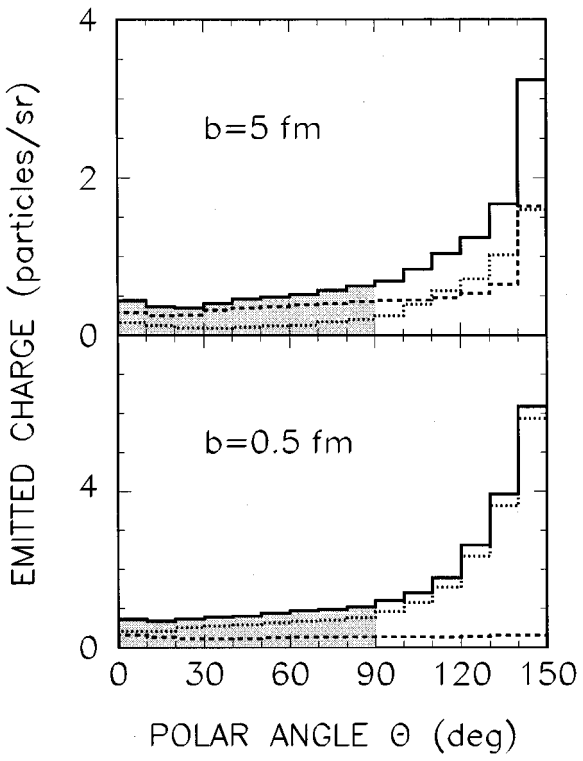

FIG. 9. Calculated angular distributions of charged particles relative to the QP (fast source) at t_{∞}. Shown are prompt charged particles (dotted histograms), delayed charged particles (dashed histograms), and the sum of all charged particles (solid histograms). The contribution of the forward moving particles is hatched. The top panel is for semiperipheral ($b=5$ fm) and the bottom panel for central ($b=0.5$ fm) collisions.

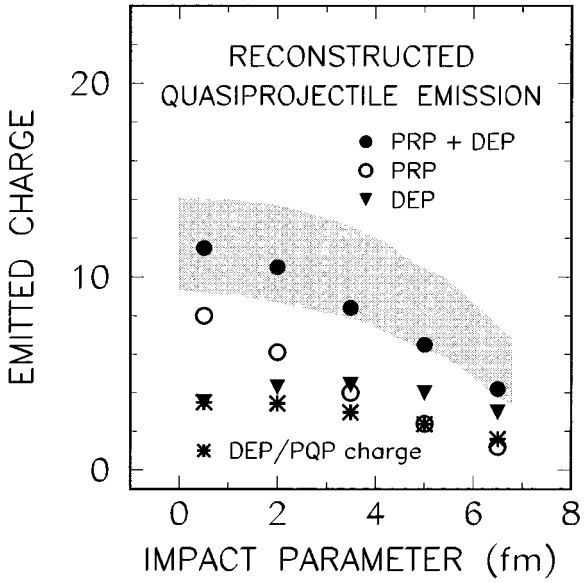

FIG. 10. Reconstructed charge ''emitted by PQP'' as a function of impact parameter. Open circles show the contribution of the prompt component (coming from the midrapidity source prior to the breakup of the PQT and the PQP), filled inverted triangles of the delayed component (the genuine PQP emission), and filled circles show the sum of both components. Stars show the DEP divided by the PQP charge and normalized to the $b=0.5$ DEP value. The hatched area represents the experimental multiplicity. The lower edge is exclusively due to the contribution of the $Z=1$ and 2 particles, whereas the upper edge includes all detected species. For further details, see the text.

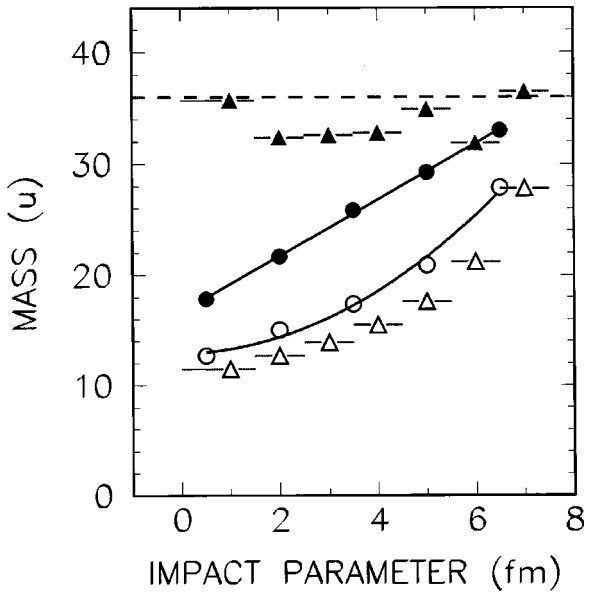

FIG. 11. Dependence of the mass of the cold QP (open symbols) and the PQP (filled symbols) on impact parameter. Triangles show the experimental and circles the theoretical results. The dashed horizontal line shows the projectile mass (^{36}Ar). The solid line and the curve through calculated values are drawn to guide the eye and are due to the fit with a linear and a quadratic function, respectively. The calculated values are scaled by a factor of 0.9 to account for the different Ar isotope used in the simulation (^{40}Ar).

rapidity contamination falls rapidly with b, whereas the Fermi-jetlike emission is roughly b independent: The PEP's attain 40% of the PRP's for peripheral collisions. The true PQP emission (DEP's) is almost b independent, exhibiting an insignificant maximum for semicentral collisions. The DEP multiplicity divided by the charge of the PQP is a quantity proportional to the average PQP excitation energy per nucleon. This quantity displays a regular decrease with b (stars), demonstrating that the PQP excitation energy increases with centrality, though this increase is not substantial. From the relative contribution of DEP's to the total reconstructed multiplicity one may deduce that $E^{\star}/A$ of PQP's cannot be high even for central collisions. The above results are in favor of the conclusion that, independently of the violence of the collision, the PQP is not very hot.

C. Mass of PQP

In the experiment, the fast evaporation residue (identified as QP) has been detected in coincidence with light particles allowing, via sorting of events into classes according to the degree of violence, one to attribute a mean mass of the cold QP to each impact-parameter bin [9,38]. From the known multiplicity of emitted particles and the mass of the QP residue, it is straightforward to reconstruct the mass of the PQP by using the procedure described in the preceding subsections. The contribution of undetected neutrons must, however, be estimated. In Fig. 11 open triangles show the measured QP residue mass as a function of b [9]. The experimentally reconstructed mass of the PQP is shown by filled triangles [9]. These values suggest that, independently of b, the PQP mass is very close to the projectile mass (dashed line). The calculated QP mass at t_{end} (open circles) agrees reasonably well with experimental findings. In particular, the calculation closely follows the experimentally observed regular, close to quadratic, rise of the QP residue mass with b. On the contrary, the PQP mass determined by the simulation at the instant t_{sep} (filled circles), when the colliding system breaks into PQT and PQP, differs substantially from the values extracted in the experimental analysis. The calculated PQP mass grows linearly with b. In central collisions, the discrepancy is as large as 18 mass units: The experimentally reconstructed PQP mass equals the projectile mass and for the PQP mass the simulation gives about half of that value, the other half of the projectile mass being evacuated by prompt emission. For peripheral collisions, the prompt emission becomes a small portion of the total emission (cf. Fig. 10) and the theory and experiment give the same values for the PQP mass.

VI. DISCUSSION AND CONCLUSIONS

We have studied the collision of ^{40}Ar + ^{27}Al at 65 MeV/nucleon theoretically by simulating it with the semiclassical Landau-Vlasov transport model. The results of the LVM simulation agree rather well with the global experimental distributions of invariant cross sections [9] and average rapidity distributions [30,38]. The experimental and theoretical estimates of the total forward emission in the QP reference frame are also in fair agreement. These favorable quantitative comparisons allow us to rely on our model to gain insight into the dynamics of BDC's. By a meticulous dynamical analysis of emitted charged particles, the simulation suggests the following.

(i) For our light system, a weak pre-equilibrium emission occurs with three distinct components: two Fermi-jetlike components at the target and the projectile rapidity, and a midrapidity component. The pre-equilibrium emission remains weak over the whole impact parameter range and does not exceed 15% of the total emission.

(ii) Before the birth of the QT and the QP, there is an abundant prompt emission ($t<80$ fm/c) coming unambiguously from the overlapping zone between the two colliding partners. This emission reminds us of the fireball participant particles from the participant-spectator collision model defined for higher energies. Negligible in peripheral collisions, these promptly emitted particles amount up to 75% of the total emission in the most central collision. Mainly located at midrapidity, this emission covers the whole accessible rapidity range of the collision. Thus it contaminates the forward hemisphere of the QP reference frame. In the analysis of experimental data, this portion of phase space is entirely attributed to the QP deexcitation [9,28]. The contamination of the forward moving particles by the prompt emission is impact-parameter dependent and varies between 28% (peripheral collisions) and 70% (central collisions). The above observation has an essential impact on the excitation energy of PQT and PQP. Indeed, the excitation energy, experimentally estimated using a calorimetric method, is calculated by summing up the kinetic energies of all these forward emitted particles, taking into account the mass balance. The result is multiplied by two, assuming a forward-backward symmetry

of the QP emission. An identical calorimetric analysis carried out with the genuine PQP deexcitation products would lead to a sensible reduction of the PQP excitation energy. The reduction of the PQP excitation energy is, besides smaller multiplicity, caused by the lower average speed of delayed particles. From our calculation, however, it turns out that it is virtually impossible to distinguish the prompt and the delayed component in the experimental data.

(iii) The last stage of the collision corresponds to the emergence of the PQT and PQP, which can, in a certain way, be identified as spectator nuclei of the reaction. Owing to the experimentally available results, only the PQP has been studied. The multiplicity of particles that are emitted isotropically in the PQP reference frame is nearly b constant. However, when the mass of the PQP is accounted for, it turns out that the smaller the impact parameter, the hotter the PQP. Our LVM simulation suggests that in the analysis of experimental violent collisions both the mass of the PQP and the amount of particles emitted by it have been largely overestimated [9,28].

By increasing the incident energy, the accessible rapidity domain becomes wider and wider. For higher energies, therefore, the participant and the spectator particles are clearly separated. Below 100 MeV/nucleon, the main difficulty comes from the entire mixing of these two components. However, for the most central collisions where participant particles govern the emission process, the study of the properties of the participant zone is of prime interest. At higher energies the central collisions are currently under extensive study [45] and similar investigations are needed at energies below 100 MeV/nucleon.

ACKNOWLEDGMENTS

Z.B. would like to express his gratitude to the Laboratoire de Physique Subatomique et des Technologies Associées and to the École des Mines de Nantes for the warm hospitality during his stay, as well as for financial support.

[1] E. Suraud, C. Grégoire, and B. Tamain, Prog. Part. Nucl. Phys. **23**, 357 (1989).
[2] J. Pochodzalla *et al.*, Phys. Rev. Lett. **75**, 1040 (1995).
[3] B. Borderie *et al.*, Phys. Lett. B **205**, 26 (1988).
[4] D. Jouan *et al.*, Z. Phys. A **340**, 63 (1991).
[5] M. F. Rivet *et al.*, in *Proceedings of the XXXI International Winter Meeting on Nuclear Physics*, Bormio, 1993, edited by I. Iori (University of Milan Press, Milan, 1993), p. 92.
[6] A. Kerambrun *et al.* (unpublished).
[7] E. Vient *et al.*, Nucl. Phys. **A571**, 588 (1994).
[8] R. Bougault *et al.*, Nucl. Phys. **A587**, 499 (1995).
[9] J. Péter *et al.*, Nucl. Phys. **A593**, 95 (1995).
[10] M. F. Rivet *et al.*, Phys. Lett. B **388**, 219 (1996).
[11] J. C. Steckmeyer *et al.*, Phys. Rev. Lett. **76**, 4895 (1996).
[12] M. F. Rivet, B. Borderie, C. Grégoire, D. Jouan, and B. Remaud, Phys. Lett. B **215**, 55 (1988).
[13] M. Colonna, M. Di Toro, V. Latora, and A. Smerzi, Prog. Part. Nucl. Phys. **30**, 17 (1992).
[14] L. Sobotka, Phys. Rev. C **50**, R1270 (1994).
[15] M. Colonna, M. Di Toro, and A. Guarnera, Nucl. Phys. **A589**, 160 (1995).
[16] F. Haddad, B. Borderie, V. de la Mota, M. F. Rivet, F. Sébille, and B. Jouault, Z. Phys. A **354**, 321 (1996).
[17] H. M. Xu, Nucl. Phys. **A568**, 365 (1994).
[18] J. Łukasik *et al.*, Phys. Rev. C **55**, 1906 (1997).
[19] J.-G. Ma *et al.*, Phys. Lett. B **388**, 219 (1996).
[20] M. Lefort and Ch. Ngô, Ann. Phys. (Paris) **3**, 5 (1978).
[21] G. D. Westfall, J. Gosset, P. J. Johansen, A. M. Poskanzer, W. G. Meyer, H. H. Gutbrod, A. Sandoval, and R. Stock, Phys. Rev. Lett. **37**, 1202 (1976).
[22] K. Hagel *et al.*, Phys. Lett. B **229**, 20 (1989).
[23] J. Péter *et al.*, Phys. Lett. B **237**, 187 (1990).
[24] J. P. Sullivan *et al.*, Phys. Lett. B **249**, 8 (1990).
[25] J. Péter *et al.*, Nucl. Phys. **A538**, 75c (1992).
[26] J. P. Sullivan and J. Péter, Nucl. Phys. **A540**, 275 (1992).
[27] W. Q. Shen *et al.*, Nucl. Phys. **A551**, 333 (1993).
[28] D. Cussol *et al.*, Nucl. Phys. **A561**, 298 (1993).
[29] S. C. Jeong *et al.*, Nucl. Phys. **A604**, 208 (1996).
[30] J. C. Angélique *et al.*, Nucl. Phys. **A614**, 261 (1997).
[31] B. Remaud, F. Sébille, C. Grégoire, L. Vinet, and Y. Raffray, Nucl. Phys. **A447**, 555c (1985).
[32] F. Sébille, G. Royer, C. Grégoire, B. Remaud, and P. Schuck, Nucl. Phys. **A501**, 137 (1989).
[33] C. Grégoire, B. Remaud, F. Sébille, L. Vinet, and Y. Raffray, Nucl. Phys. **A465**, 317 (1987).
[34] B. Remaud, C. Grégoire, F. Sébille, and P. Schuck, Nucl. Phys. **A488**, 423 (1988).
[35] D. Idier, M. Farine, B. Remaud, and F. Sébille, Ann. Phys. (Paris) **19**, 159 (1994).
[36] F. Haddad, G. Royer, F. Sébille, and B. Remaud, Nucl. Phys. **A572**, 459 (1994).
[37] P. Abgrall, F. Haddad, V. de la Mota, and F. Sébille, Phys. Rev. C **49**, 1040 (1994).
[38] J.-C. Angélique, Ph.D. thesis, University of Caen, 1993.
[39] G. Bizard, A. Drouet, F. Lefèbvres, J. P. Patry, B. Tamain, F. Guilbault, and C. Lebrun, Nucl. Instrum. Methods Phys. Res. A **244**, 489 (1986).
[40] A. Péghaire *et al.*, Nucl. Instrum. Methods Phys. Res. A **295**, 365 (1990).
[41] J. Péter *et al.*, Nucl. Phys. **A519**, 611 (1990).
[42] Z. Basrak, P. Eudes, P. Abgrall, F. Haddad, and F. Sébille, Nucl. Phys. A, in press.
[43] V. Metivier, private communication.
[44] B. Borderie *et al.*, Phys. Lett. B **388**, 224 (1996).
[45] J. P. Alard *et al.*, Phys. Rev. Lett. **69**, 889 (1992); S. C. Jeong *et al.*, *ibid.* **72**, 3468 (1994); M. Petrovici *et al.*, *ibid.* **74**, 5001 (1995); M. Dželalija *et al.*, Phys. Rev. C **52**, 346 (1995); V. Ramillien *et al.*, Nucl. Phys. **A587**, 802 (1995); W. Reisdorf *et al.*, *ibid.* **A612**, 493 (1997).